

# SCIENTIFIC REPORTS



OPEN

## Targeted gold-coated iron oxide nanoparticles for CD163 detection in atherosclerosis by MRI

Received: 24 June 2015  
Accepted: 09 October 2015  
Published: 30 November 2015

Carlos Tarin<sup>1,\*</sup>, Monica Carril<sup>2,3,\*</sup>, Jose Luis Martin-Ventura<sup>1</sup>, Irati Markuerkiaga<sup>4</sup>, Daniel Padro<sup>4</sup>, Patricia Llamas-Granda<sup>1</sup>, Juan Antonio Moreno<sup>1</sup>, Isabel Garcia<sup>2,5</sup>, Nuria Genicio<sup>2</sup>, Sandra Plaza-Garcia<sup>4</sup>, Luis Miguel Blanco-Colio<sup>1</sup>, Soledad Penades<sup>2,5</sup> & Jesus Egido<sup>1</sup>

CD163 is a membrane receptor expressed by macrophage lineage. Studies performed in atherosclerosis have shown that CD163 expression is increased at inflammatory sites, pointing at the presence of intraplaque hemorrhagic sites or asymptomatic plaques. Hence, imaging of CD163 expressing macrophages is an interesting strategy in order to detect atherosclerotic plaques. We have prepared a targeted probe based on gold-coated iron oxide nanoparticles vectorized with an anti-CD163 antibody for the specific detection of CD163 by MRI. Firstly, the specificity of the targeted probe was validated *in vitro* by incubation of the probe with CD163(+) or (−) macrophages. The probe was able to selectively detect CD163(+) macrophages both in human and murine cells. Subsequently, the targeted probe was injected in 16 weeks old apoE deficient mice developing atherosclerotic lesions and the pararenal abdominal aorta was imaged by MRI. The accumulation of probe in the site of interest increased over time and the signal intensity decreased significantly 48 hours after the injection. Hence, we have developed a highly sensitive targeted probe capable of detecting CD163-expressing macrophages that could provide useful information about the state of the atheromatous lesions.

Atherosclerosis is a complex disease that involves chronic inflammation and remodelling processes that may lead to the stenosis of the aorta. It can slowly progress over decades but under certain circumstances, it can either grow quickly or destabilize, leading to an ischemic event<sup>1</sup>. Its high morbidity and associated mortality have made atherothrombosis one of the leading causes of death in the developed world. Consequently, a large amount of resources are spent every year trying to improve its diagnosis, prognosis and treatment with the purpose of preventing a fatal event<sup>1,2</sup>.

CD163 is a membrane receptor which functions primarily as a hemoglobin (Hb) scavenger receptor, removing the complex hemoglobin-haptoglobin from the plasma and avoiding the toxic effects of free Hb. The role of CD163 has been widely studied and linked with inflammation through its function of removing pro-inflammatory ligands such as the TNF superfamily member, TWEAK<sup>3</sup>. It has been described that CD163 is expressed by the monocytic-macrophage lineage, although monocytes have a modest expression level that is increased when they acquire macrophage characteristics<sup>3</sup>. Macrophages

<sup>1</sup>Laboratorio de Patología Vascular y Renal. IIS Fundación Jiménez Díaz, Universidad Autónoma. Av. Reyes Católicos 2, 28040, Madrid, Spain. <sup>2</sup>Laboratorio de Gliconanotecnología. Biofunctional Nanomaterials Unit. CIC biomaGUNE. Paseo Miramón, 182, 20009, San Sebastián, Spain. <sup>3</sup>Ikerbasque, Basque Foundation for Science, 48011, Bilbao, Spain. <sup>4</sup>Molecular Imaging Unit, CIC biomaGUNE, Paseo Miramón 182, 20009, San Sebastián, Spain. <sup>5</sup>Biomedical Research Networking Center in Bioengineering, Biomaterials and Nanomedicine (CIBER-BBN), Paseo Miramón 182, 20009, San Sebastián, Spain. \*These authors contributed equally to this work. Correspondence and requests for materials should be addressed to J.E. (email: jegido@idcsalud.es) or S.P. (email: spenades@cicbiomagune.es)

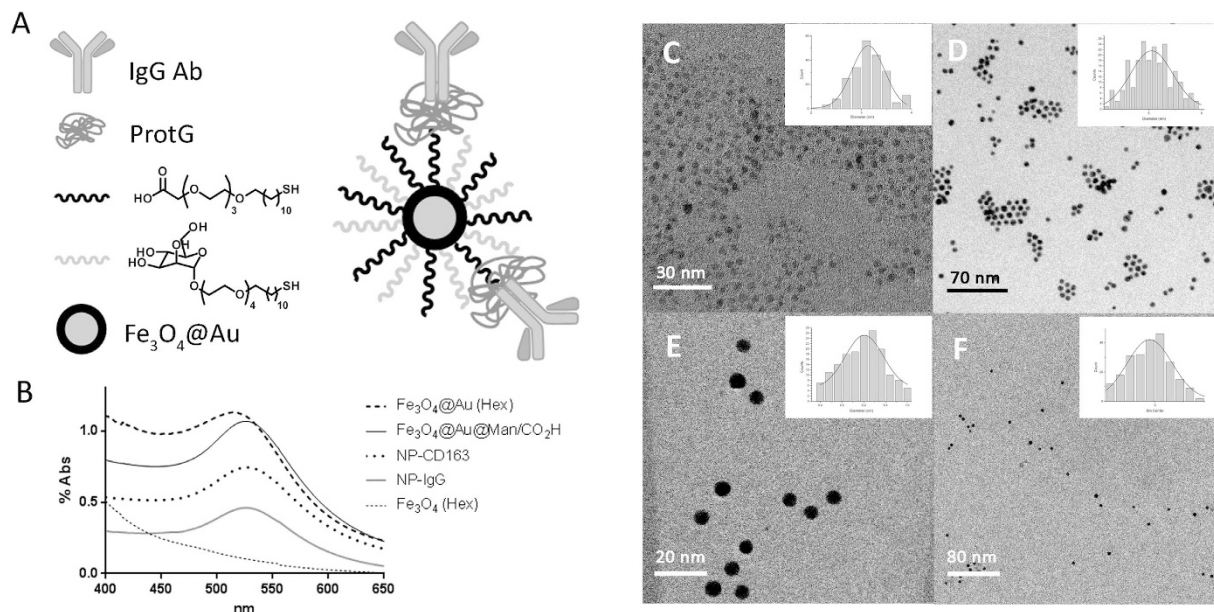


**Figure 1. Characterization of glyconanoparticles.** (A) Schematic representation of the nanoparticles. (B) UV-Vis spectra of all nanoparticles showing the appearance of the characteristic plasmon of gold. Due to their different solubilities,  $\text{Fe}_3\text{O}_4$  NPs and  $\text{Fe}_3\text{O}_4@Au$  NPs were measured in hexane solution, whereas the rest were measured in water. (C) TEM micrograph and histogram of  $\text{Fe}_3\text{O}_4$  NPs. (D) TEM micrograph and histogram of  $\text{Fe}_3\text{O}_4@Au$  NPs. (E) TEM micrograph and histogram of  $\text{Fe}_3\text{O}_4@Au@Man/CO_2H$  NPs. (F) TEM micrograph and histogram of NP-CD163.

are one of the main inflammatory cells that play key role in the development and progression of atheroma plaque<sup>4</sup>. Studies performed in atherosclerosis have shown that CD163 is expressed by anti-inflammatory M2-macrophages instead of pro-inflammatory M1-macrophages and its expression is increased at inflammatory sites, specially in plaques at sites of hemorrhage<sup>5,6</sup> or in asymptomatic plaques<sup>7</sup> while healthy aortas do not contain or contain few CD163 (+) cells<sup>8,9</sup>.

Magnetic resonance imaging (MRI) has gained relevance in cardiovascular pathology detection because of its good spatial resolution and average contrast agent sensitivity<sup>10</sup>. The development of new contrast agents that provide more than an imaging enhancement is one of the main hot topics in MRI development nowadays. In the field of contrast enhanced imaging of atherosclerosis, the detection of the plaque presence is no longer enough and efforts have been focused on providing improved information, in a non-invasive way, about the molecular composition and/or the state of the plaque. Targeting of macrophages (usually total population or M1 fraction) with  $T_1$  or  $T_2$  contrast agents is a frequent strategy for atherosclerosis imaging by magnetic resonance<sup>11</sup>, either by passive labelling<sup>12–14</sup> or by active targeting of membrane receptors with vectorized probes<sup>15–20</sup>. Nano-sized superparamagnetic iron oxide probes have been previously explored as  $T_2$  contrast agents for atheroma plaque imaging<sup>12–15,21</sup>. Among them, gold-coated iron oxide nanoparticles (NP) are particularly stable and versatile platforms. The gold coating protects the magnetite core from oxidation and allows for easy and practical functionalization of the nanoparticle surface by using thiol-ending ligands<sup>22</sup>. Indeed, gold-coated iron oxide nanoparticles vectorized with antibodies have been successfully prepared and validated as contrast agents both *in vitro* and *in vivo* in the targeting of different types of cells<sup>23–25</sup>. Herein, we prepared gold-coated iron oxide nanoparticles functionalized with antibodies against CD163 as a  $T_2$  contrast agent for the detection of M2-macrophages. Such probe was able to selectively bind to CD163-expressing macrophages *in vitro* in human and murine cells, as well as *in vivo* in a murine model of atherosclerosis. We demonstrated the ability of our probe to detect CD163 in the pathological tissue, as well as its versatility to be vectorized with immunoglobulin-G type (IgG) antibodies of our election<sup>23–25</sup>.

## Results

**Characterization of nanoparticles.** The prepared nanoparticles consisted of a gold-coated iron oxide core covered with thiol ligands bearing either a mannose or a carboxylic acid. ProtG was covalently linked through a peptide bond to the carboxylic moieties and IgG antibodies subsequently grafted onto them (Fig. 1A). Bradford analysis of the unbound protG or antibody found in each step of the functionalization showed that the amount of protG-IgG complex on each nanoparticle ranged from 1 to 2 units. Further evidence of the grafting of the antibodies on the nanoparticles was obtained by SDS-PAGE gels of digested nanoparticles which showed the typical 2 bands of IgG antibodies, at 25 kDa and

50 KDa for the light and heavy chains, respectively (See supplemental Figure S4)<sup>23</sup>. TEM micrographs showed that the average diameter of iron oxide core was 3.2 nm, which increased up to 6.1 nm after the gold coating process (Fig. 1C–F). UV-Vis spectra were measured and as expected the characteristic plasmon resonance band of gold at around 520 nm appeared in all nanoparticles after the gold coating process (Fig. 1B). Gold and iron content was obtained by ICP-OES (Inductively coupled plasma - optical emission spectroscopy) analysis on Fe<sub>3</sub>O<sub>4</sub>@Au@Man/CO<sub>2</sub>H NPs and it was found to be 59.3 ± 0.8% and 4.03 ± 0.05% in weight, respectively. Relaxivity measurements were performed at 11.7 T and room temperature resulting in  $r_2$  and  $r_1$  values of 160 mM<sup>-1</sup>s<sup>-1</sup> and 10 mM<sup>-1</sup>s<sup>-1</sup>, respectively. The full characterization of these nanoparticles, as superparamagnetic materials and contrast agents, has been previously described by our group<sup>22–26</sup>.

As part of the characterization of the NPs cell viability, toxicological profile, excretion and biodistribution studies were performed using NP-CD163(m). Cytotoxicity was not detected on RAW264.7 cell cultures incubated with increasing amounts of the tested probe (See supplemental Figure S5). In addition, the biochemical profiles of the control and the injected groups and were very similar. Urea and blood urea nitrogen levels were decreased at 24 hours after NP-CD163(m) injection, showing a better kidney function. Alkaline phosphatase activity (AP) was increased at 24 hours after injection but other metabolic liver enzymes and related metabolites such as bilirubin were similar to the control group. Also this increase of AP activity diminished to normal range at 48 hours post-injection (See supplemental Table S1). In addition, histopathological analysis was performed comparing tissue sections (stained with hematoxylin-eosin) between the control and injected groups no differences were observed (See supplemental Figure S6). Post-mortem gold content analysis of main organs by ICP-OES 48 hours after injection showed that NP-CD163(m) accumulated mainly in the liver (below 10% of the injected dose), followed in decreasing order by accumulation in spleen, lung and kidney (less than 0.5% of the injected dose for each tissue). At that time point, NPs were not detected neither in serum nor in urine by ICP-OES. Aorta of ApoE mice that have not developed atheroma plaques was also examined showing non-detectable accumulation of probe (See supplemental Figure S7). Gold deposits were detected by gold staining in tissue sections obtained from several organs, which was in agreement with the results obtained by ICP-OES (See supplemental Figure S8).

**Binding of nanoparticles to CD163, *in vitro* models.** The incubation of cells that expressed (+) or not (–) CD163 (Fig. 2A,D) with the targeted or control probes showed that the NPs bearing the anti-CD163 antibody could selectively detect CD163 expressing macrophages (Fig. 2B–C, E–F). In both human and murine CD163 (+) cells incubated with NP-CD163, there was a significant decrease in the T<sub>2</sub> values with respect to CD163 (–) macrophages incubated with the same probe ( $p < 0.05$  either THP-1 or mouse peritoneal macrophages) (See Supplementary tables S1–S6 for statistical details). Likewise, T<sub>2</sub> values were significantly lower than those for the same cells incubated with the NP-IgG control probe compared with NP-CD163 ( $p < 0.001$  in THP-1 cell line and  $p < 0.01$  in mouse peritoneal macrophages). Incubation with increasing amounts of free antibody blocked the targeting of CD163 by the NP-CD163 probe with a T<sub>2</sub> values similar to that of cells not expressing CD163 or those that were incubated with control probe. This fact showed the specificity of the vectorized probe to target CD163 and excluded unspecific signal due to the probe.

***In vivo* CD163 detection in a murine model.** ApoE<sup>–/–</sup> and wild type mice were both injected in separate experiments with either NP-CD163(m) or NP-IgG(m) and the pararenal abdominal aorta was imaged at four time points: before the injection and at 1, 24 and 48 hours post-injection. No differences were seen at 1 hour post-injection (data not shown), but a signal decrease in the aortic wall was observed in apoE<sup>–/–</sup> mice injected with NP-CD163 ( $n = 9$ ) over time with respect to the pre-injection signal. At 24 hours there was a signal decrease that became significant at 48 hours after the injection ( $p < 0.01$ ). Conversely, when the same type of mice were injected with the control probe NP-IgG(m) there were not significant signal variations over time or in healthy mice (See Supplementary tables S7–S9 for statistical details). Likewise, the wall signal intensity did not vary compared to pre-injection signal in the case of wild type mice injected with either NP-CD163(m) or NP-IgG(m) (Fig. 3).

Finally, 4 of the apoE<sup>–/–</sup> mice that were injected with NP-CD163 were scanned in the MRI 6 days after the injection to study the clearance of the nanoparticles, and a recovery of the signal comparable to pre-injection signal intensity was observed (Figure S5 in supplemental material).

**Immunohistochemistry validation.** The histology of the apoE<sup>–/–</sup> aortas, harvested after MRI scan, showed that all the mice had atherosclerotic lesions in the MRI scanned area (Fig. 4) with an average size of 50,000 ± 14,000 μm<sup>2</sup>. The plaques in the aortic wall were composed by a layer of smooth muscle cells (Fig. 4A) with small lipid deposits (oil red staining, Fig. 4B) and with the presence of infiltrated macrophages (CD68, Fig. 4C). MRI results were confirmed in the atherosclerotic mice samples by CD163 (Fig. 4D), and CD68 staining. The incubation with an isotype-matched immunoglobulin was used as a negative control, showing the specificity of the immunohistochemistry (Supplemental Figure S6).

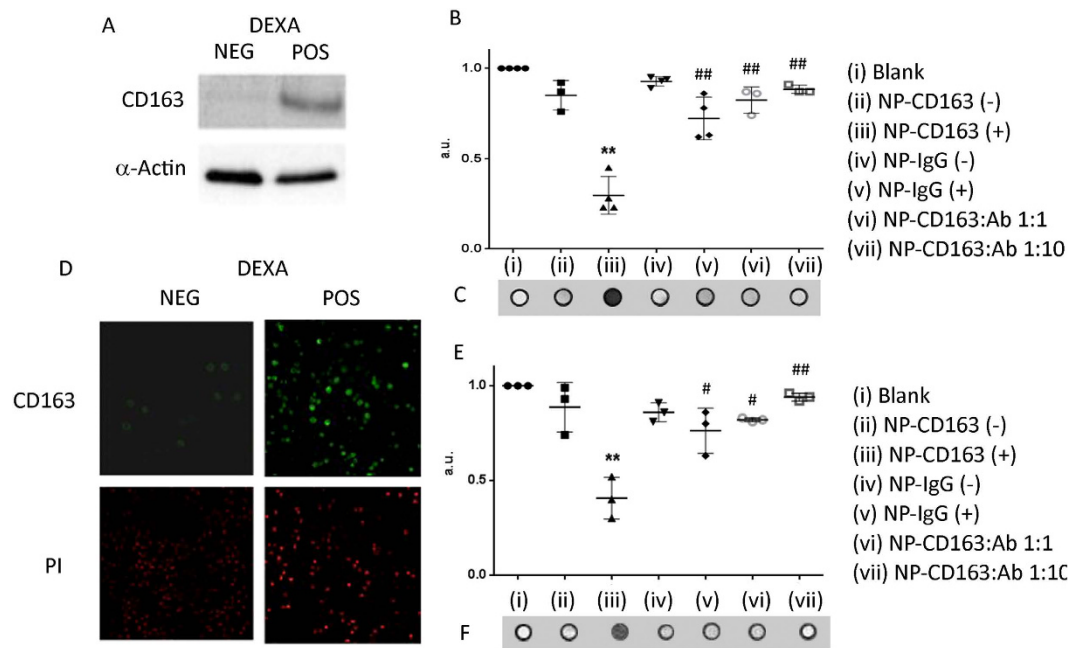


**Figure 2. CD163 detection in *in vitro* models.** (A) Western blot of CD163 expression and  $\alpha$ -actin (loading control) in THP-1 macrophages cell lysates with or without dexamethasone treatment for 24 hours. (B) Graph showing the normalized  $T_2$  values obtained from MRI images of human macrophages CD163 (+) and CD163 (-) incubated with NP-CD163(h) and NP-IgG(h),  $n = 3$ . All the replicates were normalized to the blank (cells that have not been incubated with any nanoparticles). The error bars shows the SEM.  $\$p < 0.05$  versus Blank;  $*p < 0.05$ ,  $**p < 0.01$  and  $***p < 0.001$  versus NP-CD163(+). (C) Representative MRI phantoms of human macrophages CD163 (+) and CD163 (-) incubated with NP-CD163(h) and NP-IgG(h). (D) Immunodetection of CD163 expression in murine macrophages with or without dexamethasone treatment. Propidium iodide (PI) was used for nuclei staining. (E) Graph showing the normalized mean value obtained from MRI images of murine macrophages CD163 (+) and CD163 (-) incubated with NP-CD163(m) and NP-IgG(m),  $n = 3$ . All the replicates were normalized to the blank (cells that have not been incubated with any nanoparticles). The error bars shows the SEM.  $$$p < 0.01$  versus Blank;  $*p < 0.05$  and  $**p < 0.01$  versus NP-CD163(+);  $\#p < 0.05$  versus Ab 1:1. (F) Representative MRI phantoms of murine macrophages CD163 (+) and CD163 (-) incubated with NP-CD163(m) and NP-IgG(m).

## Discussion

Imaging macrophages in atherosclerosis is an appealing strategy since they play an important role in the development, growth and rupture of atherosclerotic plaque. In particular, the use of targeted probes specifically directed to the detection of subtypes of macrophages could provide useful information on the composition of the plaque. For these reasons, the use of a targeted probe detection of CD163-expressing macrophages in atherosclerosis by MRI could be of interest, because these types of macrophages, although not exclusively, are accumulated in hemorrhaged or asymptomatic plaques<sup>5,7</sup>.

Iron oxide nanoparticles are an alternative to gadolinium based contrast agents for patients with renal disorders due to nephrogenic systemic fibrosis that the gadolinium may induce<sup>27,28</sup>. Moreover, by coating those iron oxide nanoparticles with gold we achieved a very versatile platform due to the easy functionalization of the NP surface by using thiol-ending ligands taking advantage of the stability of gold-sulphur bond. Hence, following an established procedure we were able to successfully prepare and characterize gold-coated iron oxide nanoparticles linked to anti-CD163 antibodies. Given their high specificity and availability against many proteins or their modifications, antibodies have been successfully used as vectors for the targeting of many proteins, also in atherosclerosis<sup>29</sup>. The oriented grafting of IgG antibodies on the nanoparticles by the Fc leaving the Fab exposed for recognition was a challenge that was overcome by the use of protG. Such protein is known to bind to IgG antibodies in the desired oriented manner<sup>23</sup>. The amount of protG-antibody complex ranged from 1 to 2 units per nanoparticle, which is a desirable amount to ensure that a greater number of nanoparticles link to the receptors. This platform may also be able to link any other antibody binding proteins (A, L or recombinant A/G) allowing also the conjugation of non-IgG antibodies that would potentially enable us to vectorized the probe with any type of antibody.

Subsequently, the probe was tested *in vitro* by incubation of the targeted probe (NP-CD163) and the negative control probe (NP-IgG) with both CD163 (+) and (-) macrophages. The same trend was observed in both human and mice cells and a significant decrease of the  $T_2$  values were observed when NP-CD163 was incubated with macrophages expressing CD163, whereas the  $T_2$  value did not decrease

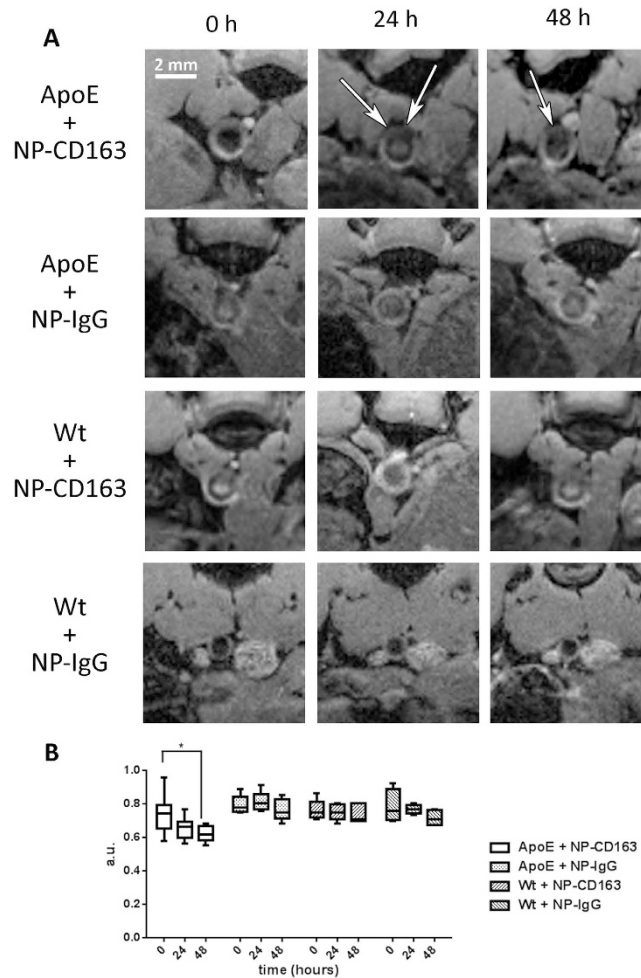


**Figure 3. Plaque detection in apoE<sup>-/-</sup> mouse model.** (A) Representative magnetic resonance images obtain before (0h) and after (24h, 48h) the injection of each type of nanoparticles. The white arrows point at slightly darker areas with respect to the pre-injection images in the case of apoE<sup>-/-</sup> mice injected with NP-CD163(m). (B) Graph showing the normalized mean value of the abdominal aortic wall for apoE<sup>-/-</sup> and wild type mice injected with either NP-CD163(m) or NP-IgG(m) at 0, 24 and 48 hours. The error bars represent the SEM. \*p < 0.05, \*\*p < 0.01 and \*\*\*p < 0.001 versus apoE + NP-CD163 t = 48h.

in a significant manner when the same cells were incubated with the control probe NP-IgG. From these data we concluded that the probe specifically targeted macrophages that expressed CD163, but in order to prove that the specificity of the nanoparticle was due to CD163 receptor recognition we performed inhibition experiments incubating with increasing concentration of free antibody before probe targeting. The unlabelled antibody blocked the targeting of CD163 (+) macrophages with the NP-CD163 probe both in human and in mice cells. It is noteworthy that one equivalent of free antibody was able to block completely the NP-CD163 T<sub>2</sub> signal. This can be explained because the NP-CD163 probe is more steric hindered than the free antibody and/or the link of the antibody to the nanoparticle might decrease the affinity for its target. Additional control experiments were performed to exclude a potential mannose-directed binding of the NPs to macrophages. For this purpose NPs without ProtG and antibodies were incubated with both CD163 (+) and (-) cells and the binding analyzed by MRI. Those NPs bound abundantly and indiscriminately to both types of cells due to the presence of mannose receptors (data not shown), however, when the NPs were functionalized with IgG antibodies we only detected significant binding when NP-CD163 was incubated with CD163 (+) cells (Fig. 2B,E). To sum up, all these results demonstrated that the probe was accumulated by CD163 (+) macrophages only through their interaction with the antibody. Hence the selected probe was suitable for the selective detection of M2-macrophages with respect to pro-inflammatory M1-macrophages in both human and mice cells.

Once the specificity of the probe was tested *in vitro*, the targeted and control probes were injected in mice developing atherosclerotic lesions and wild type mice as healthy controls. As shown by the images, the accumulation of probe in the site of interest increased over time and became significant 48 hours after the injection in atherosclerotic mice. The fact that the probe is not accumulated in healthy aorta

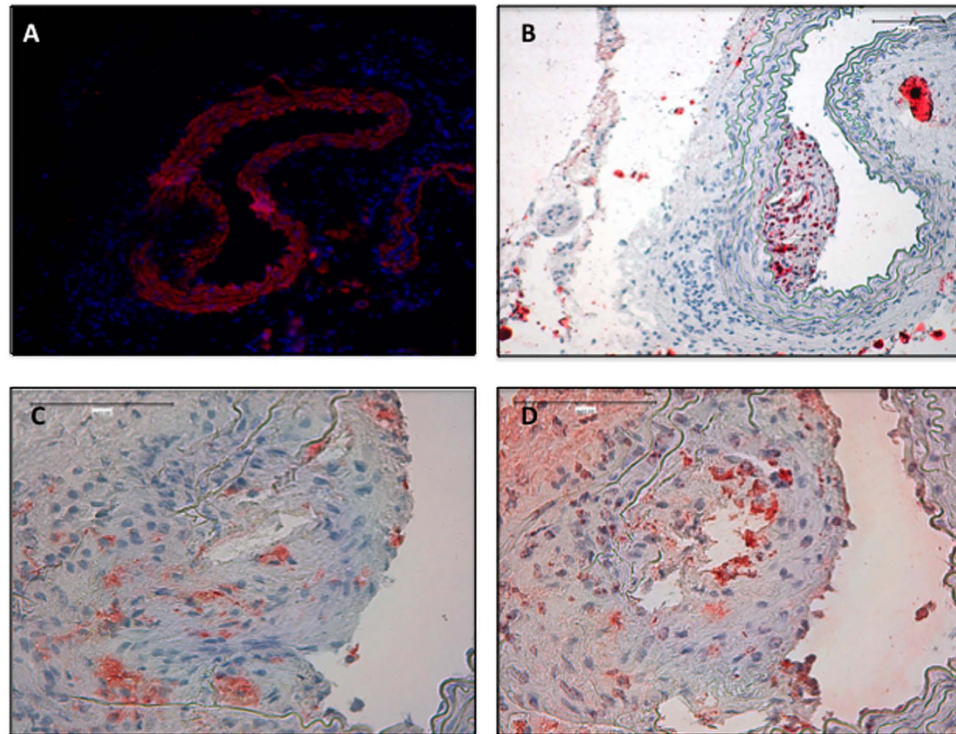


**Figure 4. Validation of the plaque presence and molecular biomarkers in apoE<sup>-/-</sup> mice.** Representative micrographs of aortic serial sections isolated from apoE<sup>-/-</sup> NP CD163(m) injected mice. (A) Vascular smooth muscle staining by  $\alpha$ -actin immunohistochemistry detection, (B) Lipid determination by Oil red staining (C) CD68 immunohistochemistry detection and (D) CD163 immunohistochemistry detection. (n = 7).

reinforces the fact that the MRI signal is due to the specific labelling of the NP-CD163(m) probe (see supplemental Figures S7-S8). The probe is cleared in time in the aorta because its presence was not detected *via* MRI 6 days post-injection. Interestingly, none of the negative controls showed a decrease in the wall intensity signal over time. Indeed, apoE<sup>-/-</sup> mice injected with NP-IgG(m) and wild type mice injected with either NP-CD163(m) or NP-IgG(m) did not present any significant changes during 48 hours after injection with respect to the signal intensity of the aortic wall before the injection. Hence, the targeted probe designed by us seems to be able to selectively detect CD163 receptor in the aortic wall of mice presenting atherosclerotic lesions. Finally, the *in vivo* results obtained by MRI were confirmed using immunohistochemistry techniques showing the presence of atherosclerotic plaques with CD163(+) macrophages in the lesions of the mice.

In conclusion, we have proved the versatility of our construction by linking it with different antibodies. The FA-11 and M-96 antibodies linked in our construction were capable to detect CD163 *in vitro* and the M-96 antibody, recognizing the mouse CD163 receptor, linked to our NP was capable of detecting a subpopulation of macrophages in atheromatous plaques *in vivo*.

## Methods

**Antibodies.** Monoclonal anti-human CD163 (AbDserotec, MCA1853), mouse IgG1 negative control (AbDserotec, MCA928), rabbit polyclonal anti-mouse CD163 (M-96, Santa Cruz, sc-33560), rabbit IgG negative control (Santa Cruz, sc-2027), monoclonal Anti- $\alpha$  Smooth Muscle Actin (Sigma-Aldrich, A-2547), rat monoclonal anti-mouse CD68 (FA-11, Abcam, ab53444) were used for MRI, western-blot and immunohistochemistry detection.

**Cell lines and culture medium.** The human monocytic cell line THP-1 [American Type Culture Collection (ATCC), Rockville, MD] and murine peritoneal macrophages, isolated as previously described<sup>30</sup>, were cultured in RPMI (BioWittaker) supplemented with 10% FBS (BioWittaker), 2 mM L-glutamine, 100 U/ml penicillin and 100  $\mu$ g/ml streptomycin (Invitrogen). THPs were differentiated to macrophages using PMA ( $10^{-7}$  M) for 48 h. After that, THP-1 macrophages cells and murine peritoneal macrophages were treated for 24 h with dexamethasone ( $2.5 \times 10^{-7}$  M) to induce CD163 expression.

**Synthesis of gold-coated iron oxide nanoparticles, functionalization with IgG antibodies and characterization.** Hexane soluble oleic acid protected iron oxide seeds (Fe<sub>3</sub>O<sub>4</sub>@oleic NPs) and gold

coated iron oxide nanoparticles ( $\text{Fe}_3\text{O}_4@Au@oleic$  NPs) herein reported were prepared as described before following a modification of a procedure reported by Wang *et al.*<sup>22,31</sup> (Supplemental Figure S1 and S2). These nanoparticles were characterized by TEM on a JEOL JEM 2100F microscope before and after the gold coating and their composition was determined by XPS analysis on a SPECS Sage HR 100 spectrometer, also before and after the coating (Supplemental Figure S3). As previously reported, oleic acid protected gold-coated iron oxide nanoparticles ( $\text{Fe}_3\text{O}_4@Au@oleic$  NPs) underwent a ligand exchange step with a 1:1 mixture of carboxylic acid ending ligands and mannose ending ligands to yield water soluble  $\text{Fe}_3\text{O}_4@Au$  nanoparticles ( $\text{Fe}_3\text{O}_4@Au@Man/CO_2H$  NPs). These nanoparticles were characterized by TEM, UV-Vis and ICP-OES for the quantification of the gold and iron content. Subsequently, water soluble  $\text{Fe}_3\text{O}_4@Au@Man/CO_2H$  NPs were converted into targeted NPs through a peptide coupling with amine groups present in protein G (protG, Pierce® Ig Binding protein, Thermo Scientific) and further incubation of IgG antibodies with the NP-protG complex, following a two step procedure described by us for the same nanoparticles<sup>23</sup>. Both human and mouse anti-CD163 and their corresponding IgG isotype antibodies were conjugated to the NP-protG complex leading to the formation of 4 probes: NP-CD163(h) and NP-IgG(h) for human antibodies, and NP-CD163(m) and NP-IgG(m) for mouse antibodies. The amount of protG and antibody on the nanoparticles was separately determined by Bradford assay of the unbound protG and the antibody recovered in the washings after the peptide coupling and the antibody incubation, respectively, as described before<sup>23</sup>. Additionally, the presence of the antibodies was confirmed by SDS-PAGE gels (Supplemental Figure S4).

**Specificity studies of nanoparticles.** *In vitro* targeting was pursued to demonstrate the specificity of NP-CD163. In order to accomplish that, two cell lines were used, human THP-1 monocyte-macrophage cell line and isolated murine macrophages. Macrophages are able to overexpress CD163 under stimulation of dexamethasone as described in Schaer *et al.*<sup>32</sup> and its expression was validated by Western-blot or immunofluorescence (Fig. 2A).  $10^6$  human cells, expressing or not CD163, were incubated with either NP-CD163(h) or NP-IgG(h) (as antibody control) at 4 °C, employing 1.5 µg of Fe per  $10^6$  cells in 300 µL of PBS. After 1 hour the cells were centrifuged to remove the unbound NPs and several washings with PBS were performed. The incubated cells were placed in capillary tubes and allowed to form a pellet overnight at 4 °C. Those capillary tubes were inserted in agarose gel (2% w/w) to prepare phantoms for MRI. The same incubation protocol was applied to murine cells that expressed or not CD163 but using  $5 \times 10^5$  cells per incubation. Inhibition studies with both cell lines were performed with increased amounts of free antibody (1:1 and 1:10 with respect to the probe), in order to block the NP-CD163 binding to ensure that the  $T_2$ -signal obtained was due to the specificity of the antibody. All incubation and inhibition experiments were performed at least 3 times.

**Animal model.** 8 weeks old B6.129P2-apoE<sup>tm1Unc</sup>/J transgenic mice (apoE<sup>-/-</sup>, n = 5–9) as atherosclerotic model and healthy wild type mice as control (Wt, n = 3–5) (Jackson Laboratory, Bar Harbor, ME) were used for *in vivo* studies. apoE<sup>-/-</sup> mice were fed during 8 weeks with high-fat diet (TD.88137 42% Fat, Harlan Teklan, Madison, Wisconsin) to induce atherosclerosis development. Mice were anesthetized for all procedures (isoflurane 2% to 3% v/v, Baxter). The NP-CD163(m) and its negative control NP-IgG(m) were injected in a dose of 2 mg Fe/Kg mice intravenously. The institutional subcommittee (Provincial Council of Guipuzcoa) on research animal care approved all animal studies, all the studies were carried out in accordance with the approved guidelines.

**MR Imaging.** Measurements were made on an 11.7 Tesla horizontal bore BrukerBiospec 117/16 scanner (Bruker A.G., Ettlingen, Germany). The actively shielded BFG-150/90-S gradient insert (Resonance Research Inc. Ballerica, MA, USA) has a 90 mm gradient coils are capable of switching 750 mT/m within 100 µs.

**Imaging of cells phantoms.**  $T_2$  relaxation times were calculated from images obtained using a multiple spin echo sequence with equally spaced 64 echoes ranging from 10 ms to 640 ms and 12000 ms repetition time. The in plane resolution was  $133 \times 133 \mu\text{m}^2$  and the slice thickness varied between 300 µm and 500 µm in the different samples. The slice thickness was varied to avoid partial volume effects from the water above the pellet of cells, as the volume of pellet could vary from sample to sample. Each echo was acquired 8 times to improve the signal to noise ratio.

**Imaging of mice.** *In vivo* images were acquired using a respiratory-triggered flow compensated gradient recalled echo sequence. The sequence parameters were the following: TR = ~1 breathing; TE = 4 ms; FA = 30°; number of averages = 1; FOV =  $2 \times 2$  cm; in plane resolution =  $78 \times 78 \mu\text{m}$ , slice thickness = 0.5 mm. Four adjacent slabs, each containing five slices, of the pararenal abdominal aorta were acquired in each experiment with a 1 mm saturation band at 2.5 mm to suppress the downstream flow entering the imaged slices. Images of the same mice were acquired before injection and 1, 24 and 48 hours after injection.

**Histopathology and immunohistochemistry.** To validate the *in vivo* MRI imaging, equivalent sections of the scanned aortas were harvested and embedded in OCT. Serial 4-µm-thick cryostat sections

were stained either with oil red for lipid deposits detection and characterization with the following antibodies: CD163 and CD68 (macrophages), and  $\alpha$ -actin (smooth muscle cells). The secondary antibodies and ABCComplex/HRP were added and sections were stained with 3, 30-diaminobenzidine, counterstained with hematoxylin and mounted in DPX. For CD163 detection Tyramide Signal Amplification Biotin Kit (PerkinElmer, NEL700A001KT) was needed to improve signal detection. Images were taken using a Nikon Eclipse E400 microscope and Nikon ACT-1 software.

**Image analysis.** MRI and histology images were analyzed using Image J (Image J 1.47v, NIH, USA). Signal intensity of the cell pellets placed inside capillary tubes was quantified in each slice for each echo time by drawing ROIs (region of interest) on them. Subsequently a monoexponential decay curve was fitted to the obtained results to calculate T2 values in each capillary tube using Origin (OriginLab, Northampton, MA). The T2 values calculated for each cell pellet were normalized to the T2 value of the blank sample (cells without NPs) and compared among them to determine the selectivity of the probes. For the *in vivo* experiments, the aortic vessel wall and the adjacent spinal muscle were manually segmented to determine the signal-to-noise-ratio (SNR) of each. The SNR of the aortic wall was normalized to the SNR of the adjacent muscle on each slice and averaged for each animal and time point. Plaque size was quantified in two slices of two sections separated from 100  $\mu$ m and next to the pararenal aorta.

**Statistics.** Results are expressed as mean  $\pm$  SEM. The data among groups were compared by using either 1-way ANOVA followed by DMS's or Games Howell's post hoc test for multiple comparisons depending on Levene's test for homogeneity of variances. It was considered statistically significant when p-value  $\leq$  0.05.

## References

- Fuster, V. *et al.* Atherothrombosis and high-risk plaque-Part II: Approaches by noninvasive computed tomographic/magnetic resonance imaging. *J. Am. Coll. Cardiol.* **46**, 1209–1218 (2005).
- Go, A. S. *et al.* Executive Summary: Heart Disease and Stroke Statistics-2013 Update A Report From the American Heart Association. *Circulation* **127**, 143–152 (2013).
- Etzerodt, A. & Moestrup, S. K. CD163 and Inflammation: Biological, Diagnostic, and Therapeutic Aspects. *Antioxid. Redox Signal.* **18**, 2352–2363 (2013).
- Ley, K., Miller, Y. I. & Hedrick, C. C. Monocyte and Macrophage Dynamics During Atherogenesis. *Arterioscler. Thromb. Vasc. Biol.* **31**, 1506–1516 (2011).
- Stoger, J. L. *et al.* Distribution of macrophage polarization markers in human atherosclerosis. *Atherosclerosis* **225**, 461–468 (2012).
- Finn, A. V. *et al.* Hemoglobin Directs Macrophage Differentiation and Prevents Foam Cell Formation in Human Atherosclerotic Plaques. *J. Am. Coll. Cardiol.* **59**, 166–177 (2012).
- Cho, K. Y. *et al.* The Phenotype of Infiltrating Macrophages Influences Arteriosclerotic Plaque Vulnerability in the Carotid Artery. *J. Stroke Cerebrovasc. Dis.* **22**, 910–918 (2013).
- Zorzi, P., Aplin, A. C., Smith, K. D. & Nicosia, R. F. The rat aorta contains resident mononuclear phagocytes with proliferative capacity and proangiogenic properties. *J. Leukocyte Biol.* **88**, 1051–1059 (2010).
- Hasan, D., Chalouhi, N., Jabbour, P. & Hashimoto, T. Macrophage imbalance (M1 vs. M2) and upregulation of mast cells in wall of ruptured human cerebral aneurysms: preliminary results. *J. Neuroinflammation* **9** 222 (2012).
- Sadeghi, M. M., Glover, D. K., Lanza, G. M., Fayad, Z. A. & Johnson, L. L. Imaging Atherosclerosis and Vulnerable Plaque. *J. Nucl. Med.* **51**, 51S–65S (2010).
- Kanwar, R. K., Chaudhary, R., Tsuzuki, T. & Kanwar, J. Emerging engineered magnetic nanoparticulate probes for targeted MRI of atherosclerotic plaque macrophages. *Nanomedicine* **7**, 735–749 (2012).
- Ruehm, S. G., Corot, C., Vogt, P., Kolb, S. & Debatin, J. F. Magnetic resonance imaging of atherosclerotic plaque with ultrasmall superparamagnetic particles of iron oxide in hyperlipidemic rabbits. *Circulation* **103**, 415–422 (2001).
- Weissleder, R. *et al.* Ultrasmall Superparamagnetic Iron-Oxide-Characterization of a New Class of Contrast Agents for MR Imaging. *Radiology* **175**, 489–493 (1990).
- Kooi, M. E. *et al.* Accumulation of ultrasmall superparamagnetic particles of iron oxide in human atherosclerotic plaques can be detected by *in vivo* magnetic resonance imaging. *Circulation* **107**, 2453–2458 (2003).
- El-Dakdouki, M. H. *et al.* CD44 Targeting Magnetic Glyconanoparticles for Atherosclerotic Plaque Imaging. *Pharm. Res.* **31**, 1426–1437 (2013).
- Amirbekian, V. *et al.* Detecting and assessing macrophages *in vivo* to evaluate atherosclerosis noninvasively using molecular MRI. *Proc. Natl. Acad. Sci. USA* **104**, 961–966 (2007).
- Lipinski, M. J. *et al.* Macrophage-Specific Lipid-Based Nanoparticles Improve Cardiac Magnetic Resonance Detection and Characterization of Human Atherosclerosis. *JACC Cardiovasc. Imaging* **2**, 637–647 (2009).
- Yamakoshi, Y. *et al.* LDL-based nanoparticles for contrast enhanced MRI of athero plaques in mouse models. *Chem. Commun.* **47**, 8835–8837 (2011).
- Li, D. *et al.* Molecular Imaging of Atherosclerotic Plaques Targeted to Oxidized LDL Receptor LOX-1 by SPECT/CT and Magnetic Resonance. *Circ. Cardiovasc. Imaging* **3**, 464–472 (2010).
- Briley-Saebo, K. C. *et al.* Targeted molecular probes for imaging atherosclerotic lesions with magnetic resonance using antibodies that recognize oxidation-specific epitopes. *Circulation* **117**, 3206–3215 (2008).
- Briley-Saebo, K. C. *et al.* Targeted Iron Oxide Particles for *In Vivo* Magnetic Resonance Detection of Atherosclerotic Lesions With Antibodies Directed to Oxidation-Specific Epitopes. *J. Am. Coll. Cardiol.* **57**, 337–347 (2011).
- Gallo, J., Garcia, I., Padro, D., Arnaiz, B. & Penades, S. Water-soluble magnetic glyconanoparticles based on metal-doped ferrites coated with gold: Synthesis and characterization. *J. Mater. Chem.* **20**, 10010–10020 (2010).
- Garcia, I., Gallo, J., Genicio, N., Padro, D. & Penades, S. Magnetic Glyconanoparticles as a Versatile Platform for Selective Immunolabeling and Imaging of Cells. *Bioconjugate Chem.* **22**, 264–273 (2011).
- Gallo, J., Garcia, I., Genicio, N., Padro, D. & Penades, S. Specific labelling of cell populations in blood with targeted immunofluorescent/magnetic glyconanoparticles. *Biomaterials* **32**, 9818–9825 (2011).
- Elvira, G. *et al.* Live Imaging of Mouse Endogenous Neural Progenitors Migrating in Response to an Induced Tumor. *PLoS One* **7**, e44466 (2012).

26. Carril, M., Fernandez, I., Rodriguez, J., Garcia, I. & Penades, S. Gold-Coated Iron Oxide Glyconanoparticles for MRI, CT, and US Multimodal Imaging. *Part. Part. Syst. Charact.* **31**, 81–87 (2014).
27. Canavese, C. *et al.* Gadolinium-associated nephrogenic systemic fibrosis: the need for nephrologists' awareness. *J. Nephrol.* **21**, 324–336 (2008).
28. Kay, J. Nephrogenic systemic fibrosis: a gadolinium-associated fibrosing disorder in patients with renal dysfunction. *Ann. Rheum. Dis.* **67** Suppl 3, iii66–69 (2008).
29. Boekhorst, B. C. M. T., Cramer, M.-J. M., Pasterkamp, G., van Echteld, C. J. A. & Doevendans, P. A. F. M. Recent developments and new perspectives on imaging of atherosclerotic plaque: role of anatomical, cellular and molecular MRI part III. *Int. J. Cardiovasc. Imaging* **26**, 447–457 (2010).
30. Ray, A. & Dittel, B. N. Isolation of mouse peritoneal cavity cells. *J. Vis. Exp.* **35**, e1488 (2010).
31. Wang, L. Y. *et al.* Monodispersed core-shell Fe<sub>3</sub>O<sub>4</sub>@Au nanoparticles. *J. Phys. Chem. B* **109**, 21593–21601 (2005).
32. Schaer, D. J., Boretti, F. S., Schoedon, G. & Schaffner, A. Induction of the CD163-dependent haemoglobin uptake by macrophages as a novel anti-inflammatory action of glucocorticoids. *Br. J. Haematol.* **119**, 239–243 (2002).

## Acknowledgements

M.C. acknowledges to Ikerbasque, Basque Foundation for Science, for a Research Fellow Grant. We also acknowledge the support from Luis Yate from the Surface Analysis and Fabrication Platform and the members of the Animal Facility at CIC biomaGUNE. Funding: This work was funded by Spanish Government through a Plan Nacional (CTQ2011–27268), FEDER funds through the Fondo de Investigación Sanitaria (PI10/00072, PI13/00051, PI13/00395, PI13/00802, PI14/00883 and PI14/00386), CIBERDEM group, RETICS RD12/0042/0038, Programa Miguel Servet (CP10/00479) and cvREMOD CENIT project (CEN-20091044), the Basque Government through Eortek 2011 (IE11–301), and Fundacion Lilly, Spanish Society of Atherosclerosis, Spanish Society of Nephrology and Fundacion Renal Iñigo Alvarez de Toledo.

## Author Contributions

T.C. conducted the experiments with animals, immunohistochemistry characterization and wrote the paper. C.M. synthesized MRI probes, quantified MRI experiments and wrote the paper. M.-V. JL is an expert in animal models and atherosclerosis. He supervised and participated in the design of the experiments. M.I. performed MRI cell phantoms acquisition. P.D. is a MRI expert. He designed MRI protocols and supervised the data acquisition. L.-G.P. performed histology related experiments. M.J.A. performed murine macrophage isolation. G.I. and G.N. performed MRI-labelling experiments with cells. Plaza-G.S. performed MRI animal data acquisition. B.-C. LM is an expert in CD163 and atherosclerosis. He chose the antibodies, supervised and participated in the design of the experiments. P.S. and E.J. are the group leaders, coordinated the project and participated in the design of the experiments and obtained funding for this work.

## Additional Information

**Supplementary information** accompanies this paper at <http://www.nature.com/srep>

**Competing financial interests:** The authors declare no competing financial interests.

**How to cite this article:** Tarin, C. *et al.* Targeted gold-coated iron oxide nanoparticles for CD163 detection in atherosclerosis by MRI. *Sci. Rep.* **5**, 17135; doi: 10.1038/srep17135 (2015).



This work is licensed under a Creative Commons Attribution 4.0 International License. The images or other third party material in this article are included in the article's Creative Commons license, unless indicated otherwise in the credit line; if the material is not included under the Creative Commons license, users will need to obtain permission from the license holder to reproduce the material. To view a copy of this license, visit <http://creativecommons.org/licenses/by/4.0/>